Electron-phonon coupling and Raman spectroscopy in graphene

A. H. Castro Neto
Department of Physics, Boston University, 590 Commonwealth Avenue, Boston, Massachusetts 02215, USA

Francisco Guinea
Instituto de Ciencia de Materiales de Madrid, CSIC, Cantoblanco E28049 Madrid, Spain
(Received 27 November 2006; published 4 January 2007)

We show that the electron-phonon coupling in graphene, in contrast with the nonrelativistic two-dimensional electron gas, leads to shifts in the phonon frequencies that are nontrivial functions of the electronic density. These shifts can be measured directly in Raman spectroscopy. We show that depending whether the chemical potential is smaller (larger) than half of the phonon frequency, the frequency shift can negative (positive) relative to the neutral case (when the chemical potential is at the Dirac point), respectively. We show that the use of the static response function to calculate these shifts is incorrect and leads always to phonon softening. In samples with many layers, we find a shift proportional to the carrier concentration, and a splitting of the phonon frequencies if the charge is not homogeneously distributed. We also discuss the effects of edges in the problem.

DOI: 10.1103/PhysRevB.75.045404 PACS number(s): 78.30.Na, 63.20.Kr, 81.05.Uw

I. INTRODUCTION

The discovery of graphene, a thermodynamically stable two-dimensional (2D) crystal,[1] whose electronic properties, described in terms of a half-filled π-electronic band with Dirac electrons, can be controlled externally, has stirred great interest in the scientific community since the demonstration of a theoretically predicted[2,3] anomalous integer quantum Hall effect.[4,5] Unlike other 2D electronic systems, such as MOSFET heterostructures, graphene is easily accessible to optical probes. Furthermore, in contrast to ordinary semiconductors where the different types of disorder can be distinguished through the temperature dependence of the transport properties,[6] graphene does not show any strong temperature or magnetic field dependence in its electronic transport[7] that allows an easy discrimination between different types of impurities. Hence, local probes such as scanning tunneling microscopy (STM) and single electron transistor probes, will play a fundamental role in the understanding of nature the effects of disorder in graphene-based systems.

Raman spectroscopy has been one of the most successful experimental methods used to study these systems.[8–11] In particular, it has been shown that it is possible to measure the number of graphene layers on a SiO_2 substrate with great accuracy, leading to an efficient and fast method to characterize graphene *in situ*. Another interesting feature of these measurements is that, even for a single graphene layer, the phonon frequency measured in Raman shifts by a few wave numbers, from point to point in space.[8–10] Moreover, the observation of a *D* line, which is Raman forbidden in translational invariant graphene, indicates the presence of disorder in the samples at electronic scale.

We show that this Raman shift can be associated with the earlier experimental evidence for charge inhomogeneity in undoped, unbiased, graphene.[7,12] Therefore, Raman spectroscopy can be used to *map* the disorder in graphene layers, and hence, help to shed light on the nature of the disorder scattering in these materials. The understanding of the nature of impurity scattering in graphene is fundamental not only for the development of electronic devices based on carbon, but also may help to solve theoretical puzzles such as the discrepancy found between the theoretically predicted universal value of the conductivity,[13] $4e^2/(\pi h)$, and its experimentally observed[4] value of $4e^2/h$ (the so-called "mystery of the missing π"), and the absence of weak-localization effects[7] (a topic that has generated intense theoretical debate[14–20]).

In this paper we show that the shift in the phonon frequency in graphene has its origin on the polarization of the electrons due to the ion motion. Since graphene is a perfect hybrid between a metal and a semiconductor there are two contributions to the polarization function: one comes from intraband transitions and another that originates on interband transitions. We show that the simplest approximation based on the static response is incorrect and predicts a reduction of the phonon frequency (softening of the lattice). The correct dynamic response is used to calculate the phonon frequency shift and it is shown that the phonon frequency can either decrease (softening) or increase (hardening) depending on whether the phonon frequency is either larger or smaller than twice the chemical potential, respectively. We also show that the intraband dynamic response vanishes at long wavelengths in a translationally invariant graphene sheet, while the interband contribution is finite. Nevertheless, in disordered graphene we expect the intraband contribution to be of the order of the interband one, indicating that disorder is important for the measurement of the Raman shift in graphene.

The paper is organized as follows. In Sec. II we present the model for the electrons, phonons, and their coupling in graphene. Sec. III discusses the problem of the shift of the phonon frequency due to the electronic polarization in graphene and we consider both the static and the dynamic response. In Sec. IV we examine the problem of phonon frequency shifts in bilayers and multilayers within the same framework. Sec. V contains a discussion of the problem of edges in finite samples and also the main conclusions of our work. We have also included one appendix with the details of

an analytical model for the in-plane phonon modes in graphene, and also discuss the effect of defects and edges in the phonon spectra.

II. THE MODEL

In the absence of disorder the Hamiltonian for electrons and phonons in graphene can be written as $\mathcal{H}=\mathcal{H}_E+\mathcal{H}_P+\mathcal{H}_{E-P}$, where (we use units such that $\hbar=1=k_B$)

$$\mathcal{H}_E=-t_0\sum_{\langle i,j\rangle}(c^\dagger_{A,i}c_{B,j}+\text{H . c . })-\mu\sum_{i,a=A,B}c^\dagger_{a,i}c_{a,i}, \quad (1)$$

is the free electron Hamiltonian, where μ is the chemical potential, $c_{a,i}$ ($c^\dagger_{a,i}$) annihilates (creates) and electron on sublattice $a=A,B$ on site $\mathbf{R}_i$ in the honeycomb lattice (spin indices are omitted throughout the paper), and $t_0\approx 2.7$ eV is the nearest neighbor hopping energy. H_P is the phonon Hamiltonian

$$\mathcal{H}_P=\sum_{\mathbf{q},i}\omega_{\mathbf{q}i}b^\dagger_{\mathbf{q}i}b_{\mathbf{q}i}, \quad (2)$$

where $b_{\mathbf{q},a}$ ($b^\dagger_{\mathbf{q},a}$) annihilates (creates) a phonon with momentum $\mathbf{q}$, and i=TA, LA, TO, L0, are the four phonon modes.[21] In the following, we focus on the transverse optical (TO) modes near the Γ and K and K' points of the Brillouin zone. The TO band shows little dispersion with a frequency $\omega_0\approx 0.19$ eV.

We assume that the electron-phonon coupling arises from the modulation by the phonons of the carbon-carbon distance $a=1.42$ Å, which leads to a change in the nearest neighbor hopping t_0. The dependence of t_0 on distance l has been extensively studied[22,23]

$$\partial t_0/\partial l=\alpha\approx 6.4 \text{ eV Å}^{-1}. \quad (3)$$

The resulting electron-phonon interaction is

$$\begin{aligned}\mathcal{H}_{E\text{-}P}=(\partial t_0/\partial l)\sum_{\mathbf{k},\mathbf{q}}c^\dagger_{A\mathbf{k}}c_{B\mathbf{k}+\mathbf{q}}\{x_{A\mathbf{q}}[1-e^{i(\mathbf{k}+\mathbf{q})\mathbf{a}}/2-e^{i(\mathbf{k}+\mathbf{q})\cdot\mathbf{b}}/2]\\ -x_{B\mathbf{q}}[1-e^{i\mathbf{k}\cdot\mathbf{a}}/2-e^{i\mathbf{k}\cdot\mathbf{b}}/2]+(\sqrt{3}/2)y_{A\mathbf{q}}[e^{i(\mathbf{k}+\mathbf{q})\cdot\mathbf{a}}\\ -e^{i(\mathbf{k}+\mathbf{q})\cdot\mathbf{b}}]-(\sqrt{3}/2)y_{B\mathbf{q}}[e^{i\mathbf{k}\cdot\mathbf{a}}-e^{i\mathbf{k}\cdot\mathbf{b}}]\}+\text{H . c . }, \quad (4)\end{aligned}$$

where $\mathbf{a}$ and $\mathbf{b}$ are the unit vectors of the honeycomb lattice, and $x_{a\mathbf{q}}, y_{a\mathbf{q}}$ ($a=A,B$) are given by the polarization of the phonon of wave vector $\mathbf{q}$. They can be written as

$$\begin{pmatrix}x_{A\mathbf{q}}\\ y_{A\mathbf{q}}\\ x_{B\mathbf{q}}\\ y_{B\mathbf{q}}\end{pmatrix}\equiv\frac{1}{\sqrt{2M_C\omega_{\mathbf{q}}}}(b^\dagger_{\mathbf{q}}+b_{-\mathbf{q}})\begin{pmatrix}\alpha_1\\ \alpha_2\\ \alpha_3\\ \alpha_4\end{pmatrix}, \quad (5)$$

where $M_C=1.2\times 10^4 m_e$ is the carbon mass (m_e is the electron mass) and the vector $(\alpha_1,\alpha_2,\alpha_3,\alpha_4)$ is normalized to 1.

In order to obtain the polarizability of the TO mode, we use a central force model (see the Appendix) which leads to a phonon dispersion which can be calculated analytically.[24] This model is adapted from similar models for tetrahedrally bonded lattices.[25] The details of the model are described in the Appendix , where it is illustrated by some applications. The honeycomb lattice, even in the limit when the bonds are incompressible, can have shear deformations, leading to a vanishing shear modulus. Because of it, the model shows a flat transverse acoustical branch at zero energy. The optical modes, on the other hand, induce significant changes in the bond lengths. We focus here on a single optical mode, whose energy we take from experiments. The polarization is fixed by symmetry considerations. Hence, the model is needed only to describe the coupling to the electrons. The only coupling consistent with nearest neighbor tight binding model used to describe the π bands is the one that we are using.

The polarization of the nondegenerate mode at the K point in the Brillouin zone is

$$(\alpha_1,\alpha_2,\alpha_3,\alpha_4)=(1/2,i/2,-1/2,i/2) \quad (6)$$

and we have a doubly degenerate mode (a Dirac phonon) with polarizations

$$(\alpha_1,\alpha_2,\alpha_3,\alpha_4)=(1/\sqrt{2},-i/\sqrt{2},0,0),$$

$$(\alpha_1,\alpha_2,\alpha_3,\alpha_4)=(0,0,1/\sqrt{2},i/\sqrt{2}). \quad (7)$$

For comparison, the polarization of the two optical modes at the Γ point can be written as

$$(\alpha_1,\alpha_2,\alpha_3,\alpha_4)=(1/\sqrt{2},0,-1/\sqrt{2},0),$$

$$(\alpha_1,\alpha_2,\alpha_3,\alpha_4)=(0,1/\sqrt{2},0,-1/\sqrt{2}). \quad (8)$$

III. SINGLE LAYER GRAPHENE

We are interested in the modification induced by electronic transitions of the frequency of a phonon with wave vector $\mathbf{Q}$. The electronic transitions which describe these processes are given, approximately, by

$$\mathcal{H}_{\mathbf{Q}}\equiv 3\alpha/2\sum_{\mathbf{k}}c^\dagger_{A\mathbf{K}}c_{B\mathbf{K}'+\mathbf{k}}(x_{A\mathbf{Q}}-x_{B\mathbf{Q}}+iy_{A\mathbf{Q}}+iy_{B\mathbf{Q}})+\text{H . c . }, \quad (9)$$

where we assume that the main contribution arises from transitions close to the Fermi level. In this limit, we can use the continuum limit and expand the energy of the electrons around the K and K' points, leading to the Hamiltonian

$$\mathcal{H}_0=\begin{pmatrix}-\mu & v_F|\mathbf{k}|e^{i\phi_{\mathbf{k}}} & 0 & 0\\ v_F|\mathbf{k}|e^{-i\phi_{\mathbf{k}}} & -\mu & 0 & 0\\ 0 & 0 & -\mu & v_F|\mathbf{k}|e^{-i\phi_{\mathbf{k}}}\\ 0 & 0 & v_F|\mathbf{k}|e^{i\phi_{\mathbf{k}}} & -\mu\end{pmatrix}, \quad (10)$$

where $v_F=3t_0a/2\approx 6$ eV Å is the Fermi-Dirac velocity, and $\phi_{\mathbf{k}}=\arctan(k_y/k_x)$ is the angle in momentum space.

A typical diagram which describes the renormalization of the phonon propagator in second order perturbation theory is given in Fig. 1. The convolution of electronic Green's functions shown in the diagram is formally identical to the charge susceptibility of graphene

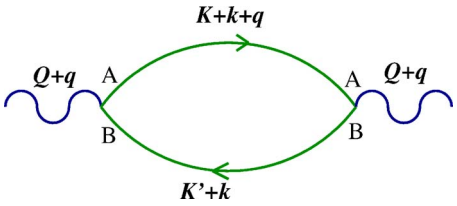

FIG. 1. (Color online) Diagram which describes the modification of the phonon propagator (wavy line) due to electron-hole transitions. See text for details.

$$\chi(\mathbf{q},\omega) = \int d^2\mathbf{k}d\omega'[G_{AA}^{\text{occ}}(\mathbf{k},\omega')G_{BB}^{\text{empty}}(\mathbf{k}+\mathbf{q},\omega+\omega') + G_{AB}^{\text{occ}}(\mathbf{k},\omega')G_{BA}^{\text{empty}}(\mathbf{k}+\mathbf{q},\omega+\omega')], \tag{11}$$

where $G_{ab}^{\text{occ}}(\mathbf{k},\omega)$ $[G_{ab}^{\text{empty}}(\mathbf{k},\omega)]$ with $a,b=A,B$ is the electronic Green's function for the occupied (empty) states. The main difference between Eq. (11) and the charge susceptibility of graphene is that the charge susceptibility includes an overlap factor which suppresses completely transitions between the valence and conduction band at $\mathbf{q}=0$.

From Fig. 1 we can immediately obtain the shift in the phonon frequency due to the polarization of the graphene layer due to particle-hole excitations

$$\delta\omega_{\mathbf{Q}} = \frac{27\sqrt{3}a^2|\alpha_1-\alpha_2+i\alpha_3+i\alpha_4|^2}{16M_C\omega_{\mathbf{Q}}}\left(\frac{\partial t_0}{\partial l}\right)^2\chi(\omega_{\mathbf{Q}},q\to 0), \tag{12}$$

where we have used that $\Omega=3\sqrt{3}a^2/2$ is the area of the unit cell.

Graphene, from the electronic point of view, is a hybrid between a metal and a semiconductor: the polarization involves not only interband excitations (as in the case of the ordinary electron gas) but also intraband excitations (as in the case of a semiconductor). The full susceptibility χ can be separated into an intraband and an interband contributions:

$$\chi(q,\omega) = \chi^{\text{inter}}(q,\omega) + \chi^{\text{intra}}(q,\omega). \tag{13}$$

The intraband contribution to the susceptibility was originally calculated by Shung for graphene in Ref. 26 and more recently it has appeared in Refs. 27–30.

A. Static approximation

A commonly used approximation on the electron gas problem is to replace the dynamical response $\chi(\omega=\omega_Q,q=0)$ by the static one: $\chi(\omega=0,q=0)$. This approximation is usually justified in ordinary metals because the Fermi energy μ is much larger than the phonon frequency so that the phonons respond to a time averaged electron distribution. In graphene, however, this is not necessarily so. In what follows we will study the effect of an static response and compare it with what happens when a dynamic response is calculated instead. We will show that these two approximations give very different results.

At finite doping, the compressibility sum rule leads to the equation

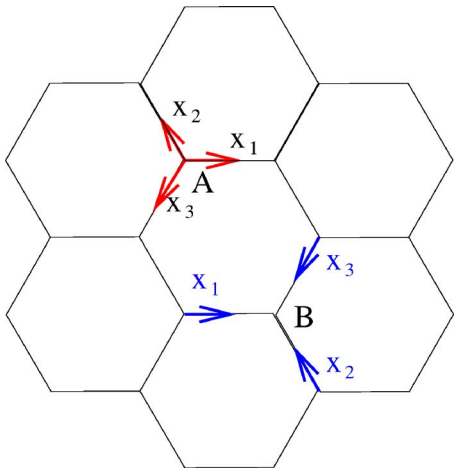

FIG. 2. (Color online) Notation used for the atomic displacements used in the text.

$$\lim_{\mathbf{q}\to 0}\chi^{\text{intra}}(\mathbf{q},\omega=0) = -D(\mu) = -\frac{2\mu}{\pi v_F^2}, \tag{14}$$

where $D(\mu)$ is the density of states at the Fermi level. The number of carriers per unit cell n_Ω is given by

$$n_\Omega = \frac{3\sqrt{3}}{2\pi}(k_F a)^2. \tag{15}$$

In addition, we have

$$\lim_{\mathbf{q}\to 0}\chi^{\text{inter}}(q\to 0,\omega=0) = -\frac{1}{\pi^2}\int_{k_F}^{\Lambda} kdk\int_0^{2\pi} d\theta\frac{\cos^2(\theta)}{\epsilon_k}. \tag{16}$$

The main contribution to the integral comes from $k\sim\Lambda$, where Λ is the high energy cutoff, so that this expression depends on details of the bands at high energies away from the Dirac point. Nevertheless, the change of the susceptibility with electronic density is independent of the cutoff and can be readily calculated:

$$\lim_{\mathbf{q}\to 0}[\chi^{\text{inter}}(\mu)-\chi^{\text{inter}}(0)] = \delta\chi^{\text{inter}}(q\to 0,\omega=0) \approx -\frac{\mu}{\pi v_F^2}. \tag{17}$$

which is of the same magnitude as the intraband shift (14).

Inserting Eqs. (14), (17), and (15) into Eq. (12), we find, in addition to a density independent shift

$$\delta\omega_{\mathbf{Q}} = -\frac{9}{\sqrt{6\pi}}\left(\frac{\partial t_0}{\partial l}\right)^2\frac{n_\Omega^{1/2}}{M_C\omega_{\mathbf{Q}}t_0}. \tag{18}$$

Expressing $\delta\omega_{\mathbf{Q}}$ (in eV) and replacing n_Ω by the density per unit area n (expressed in cm^{-2}), we find

$$\delta\omega_{\mathbf{Q}}(\text{eV}) \approx -3\times 10^{-9}n^{1/2}(\text{cm}^{-2}) \tag{19}$$

is the expression for the shift of the phonon frequency in the static approximation. For typical electron (or hole) densities, $n\approx 10^{11}-10^{12}\ \text{cm}^{-2}$, the shifts are of the order of a few wavelengths (or degrees), within experimental accuracy.

Let us first notice that this result indicates that there is a decrease of the phonon frequency, that is, a softening of the lattice. This result is generically expected on physical grounds since a high density of electrons leads to the screening of the ion-ion interactions, reducing the elastic coupling in the lattice, and hence leading to a softening of the phonons.

B. Dynamic approximation

The real part of the intra-band susceptibility is given by[30]

$$\mathrm{Re}[\chi^{\mathrm{intra}}(\omega,q\rightarrow 0)] \approx -\frac{q^2}{2\pi\omega}\left\{\frac{2\mu}{\omega}+\frac{1}{2}\ln\left|\frac{2\mu-\omega}{2\mu+\omega}\right|\right\}. \tag{20}$$

This expression is rather different from the static result (14). We note that the limits of $\omega=0$ and $q\rightarrow 0$ with $\omega\rightarrow 0$ and $q=0$ do not commute. Moreover, we clearly see that Eq. (20) changes behavior whether $\omega/(2\mu)$ is smaller or larger than one, and the susceptibility has a logarithmic singularity in $\omega=2\mu$.

For $2\mu\gg\omega$ a self-consistent calculation of the polarizability shows the existence of the two dimensional plasmon, which needs to be taken into account. We find

$$\mathrm{Re}[\chi^{\mathrm{intra}}(\omega\ll 2\mu,q\rightarrow 0)] \approx \frac{-q^2\mu}{\pi[\omega^2-\omega_{\mathrm{pl}}^2(q)]}, \tag{21}$$

where $\omega_{\mathrm{pl}}(q)=\sqrt{(2e^2\mu q)/\epsilon_0}$ is the plasmon frequency (e is the electric charge and ϵ_0 the dielectric constant of graphene). For $2\mu\ll\omega$ we find

$$\mathrm{Re}[\chi^{\mathrm{intra}}(\omega\gg 2\mu,q\rightarrow 0)] \approx \frac{4}{3\pi}\frac{q^2\mu^2}{\omega^4}. \tag{22}$$

Observe the change of sign in the expression of the susceptibility in the two limits. More importantly, one can clearly see that these expressions vanish when $q\rightarrow 0$. This effect occurs because at $q=0$ the states associated with these transitions are orthogonal. Hence, in a system with translational invariance the intraband transitions give no contribution. Nevertheless, in the presence of disorder (or a finite sample), the electron mean free path l (or the system size L) acts naively as a infrared cutoff and one would expect to see a nonzero effect. Replacing Eqs. (21) and (22) into Eq. (12), and assuming that $\omega_{\mathbf{Q}}\gg\omega_{\mathrm{pl}}$, we find

$$\delta\omega_{\mathbf{Q}}^{\mathrm{intra}}(2\mu>\omega_Q) \approx \frac{9}{2\sqrt{6\pi}}\left(\frac{\partial t_0}{\partial l}\right)^2\frac{n_\Omega^{1/2}}{M_C\omega_{\mathbf{Q}}t_0}\left(\frac{v_F q}{\omega_{\mathbf{Q}}}\right)^2, \tag{23}$$

$$\delta\omega_{\mathbf{Q}}^{\mathrm{intra}}(2\mu<\omega_Q) \approx \frac{-9\sqrt{\pi}}{\sqrt{2}}\left(\frac{\partial t_0}{\partial l}\right)^2\frac{n_\Omega^{3/2}}{M_C\omega_{\mathbf{Q}}t_0}\left(\frac{t_0 v_F q}{\omega_{\mathbf{Q}}^2}\right)^2. \tag{24}$$

Expressing $\delta\omega_{\mathbf{Q}}$ in eV, and replacing n_Ω by the density per unit area n expressed in cm^{-2}, we find

$$\delta\omega_{\mathbf{Q}}^{\mathrm{intra}}(2\mu>\omega_Q) \approx +1.4\times 10^{-6}n^{1/2}(qa)^2, \tag{25}$$

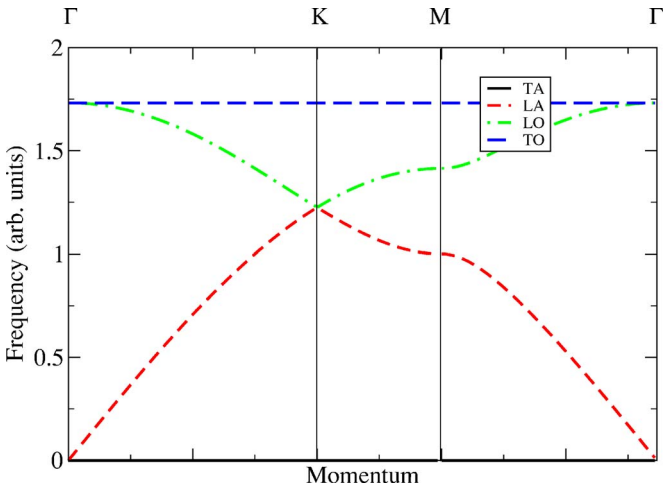

FIG. 3. (Color online) Phonon dispersion relations for the model used in the text. Continous thick (black) line: transverse acoustic; short dashed (red) line: longitudinal acoustic; dashed-dotted (green) line: longitudinal optical; long dashed (blue): transverse optical.

$$\delta\omega_{\mathbf{Q}}^{\mathrm{intra}}(2\mu<\omega_Q) \approx -1.0\times 10^{-18}n^{3/2}(qa)^2. \tag{26}$$

We stress, once again, that this shift vanishes as $q\rightarrow 0$ and hence there should be no shift in the phonon frequency due to intraband transitions in a translationally invariant graphene sheet. Nevertheless, in the presence of disorder this is not necessarily the case.

In order to include disorder in the calculation one would have to dress the fermion propagators in Fig. 1 by disorder and include vertex corrections to that diagram. These calculations are beyond the scope of this paper. Instead, we will follow a naive approach and simply introduce a cutoff in q of the order of the inverse of the electron mean free path l, which is known to be of order of 0.1 μm in these systems[7]. For typical electron (or hole) densities, $n\approx 10^{12}-10^{13}$ cm^{-2}, and $l\approx 10^3 a$ ($l\approx 0.1$ μm) the shifts are of the order of $10^{-6}-10^{-5}$ eV. For these concentrations and wavelengths, the plasmon frequency is $\omega_{\mathrm{pl}}\approx 0.01-0.04$ eV, so that the assumptions leading to Eq. (24) are justified. Notice that while for large doping, $\mu>\omega_Q/2$, the intraband contribution leads to a hardening of the phonon, for low doping, $\mu<\omega_Q/2$ there is softening of the phonon mode which depends directly on the amount of disorder in the system.

The interband susceptibility is

$$\mathrm{Re}[\chi^{\mathrm{inter}}(q\rightarrow 0,\omega)] \approx -\frac{1}{\pi}\mathcal{P}\int kdk\frac{4\epsilon_k}{\omega^2-4\epsilon_k^2}. \tag{27}$$

As in the static case, we find a large contribution which is independent of the carrier concentration and depend on the high-energy cutoff. As before, we consider only the density dependent contribution

$$\mathrm{Re}[\delta\chi^{\mathrm{inter}}(q\rightarrow 0,\omega)] \approx -\frac{\mu}{\pi v_F^2}-\frac{\omega}{4\pi v_F^2}\ln\left|\frac{\omega-2\mu}{\omega+2\mu}\right|. \tag{28}$$

The first term in this expression reproduces the static limit of χ^{inter}. The second term gives a correction which is more im-

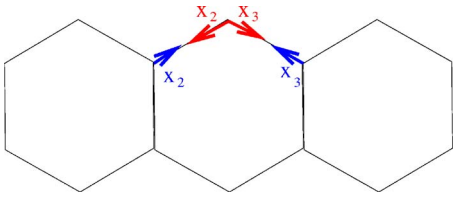

FIG. 4. (Color online) Displacements used to define the variable a_{mn} of an atom at a zigzag edge, and the variable b_{mn} at its nearest neighbor atom.

portant for $\omega \sim 2\mu$, and cancels the static contribution as $\omega_{\mathbf{Q}}/\mu \to \infty$. Comparing Eq. (20) with Eq. (28) we find that

$$\mathrm{Re}[\chi^{\mathrm{intra}}(\omega, q = \omega/v_{\mathrm{F}})] = \mathrm{Re}[\delta\chi^{\mathrm{inter}}(\omega, q = 0)], \tag{29}$$

implying, from Eq. (26), that

$$\delta\omega_{\mathbf{Q}}^{\mathrm{inter}}(2\mu > \omega_Q) \approx +3 \times 10^{-9} n^{1/2}, \tag{30}$$

$$\delta\omega_{\mathbf{Q}}^{\mathrm{inter}}(2\mu < \omega_Q) \approx -2 \times 10^{-21} n^{3/2}. \tag{31}$$

Once again, for $\mu > \omega_Q/2$, the interband contribution leads to a hardening of the phonon, while for $\mu < \omega_Q/2$ there is softening of the phonon mode. Notice, that the numerical value of the interband contribution is small for densities of order 10^{12} cm^{-2} when compared with the intraband contribution estimated in the presence of disorder. It may well be that in disordered graphene the intraband transitions dominate over the interband transitions. Hence, the final result may vary with the amount of disorder in the samples.

IV. BILAYERS

The previous analysis can be extended to a bilayer system. For simplicity, we consider here the static limit only. The model for the in-plane phonons considered before needs no changes. The shift in the phonon frequency is also given by the electronic susceptibility shown in Fig. 1, and given in Eq. (11).

In a bilayer, however, the wave functions corresponding to the low energy electronic states have a small amplitude, $a_{A\mathbf{k}} \sim \mathbf{k}|\mathbf{k}|/t_\perp$ in the orbitals hybridized through the hopping $t_\perp$ with an orbital in the next layer ($t_\perp \approx 0.3$ eV is the interlayer hopping energy). The relevant susceptibility involves a convolution of the Green's function of sites in both sublattices, so that the reduction in low energy spectral weight at the sites with a neighbor in the next layer will reduce the susceptibility.

The amplitude of an electronic wavefunction at energy $e^{i\phi_{\mathbf{k}}} \approx v_F^2 |\mathbf{k}|^2/t_\perp^2 \ll 1$ is of order $a_B \sim V^{-1/2}$, where V is the volume of the system, on sites of the sublattice not connected to the second layer, defined as sublattice B. The amplitude on sites in sublattice A, where the sites are connected to the second layer is of order $a_A \sim v_F|\mathbf{k}|/t_\perp \times a_B$. Then, the contribution to the susceptibility from the low energy electron-hole pairs is of the form

$$\chi_{\mathrm{bilayer}}^{\mathrm{intra}}(\mathbf{q}, \omega = 0) \approx \int d\mathbf{k} \frac{v_F^2 \mathbf{k}(\mathbf{k}+\mathbf{q})}{t_\perp^2} \frac{n_{\mathbf{k}+\mathbf{q}} - n_{\mathbf{k}}}{\epsilon_{\mathbf{k}+\mathbf{q}} - \epsilon_{\mathbf{k}}}. \tag{32}$$

The same suppression applies to interband transitions, as, in any case, the modulation of the hopping involves transitions from the A sublattice to the B sublattice. Using dimensional arguments, which are also valid for single layer graphene, at the neutrality point we find, $\chi_{\mathrm{bilayer}}^{\mathrm{intra}}(\mathbf{q}, \omega = 0) \propto |\mathbf{q}|^2/t_\perp$ and, at finite fillings,

$$\lim_{|\mathbf{q}| \to 0} \chi_{\mathrm{bilayer}}^{\mathrm{intra}}(\mathbf{q}, \omega = 0) \propto k_F^2/t_\perp. \tag{33}$$

As in the single layer case, the interband susceptibility includes a contribution determined by the high energy cutoff, and density dependent term, which, also on dimensional grounds, depends on density as the intraband susceptibility (33).

For the interband contribution, using the reduction in the amplitude at the A sublattice mentioned earlier, we find

$$\chi_{\mathrm{bilayer}}^{\mathrm{inter}}(\mathbf{q}, \omega = 0) \propto \frac{v_F^2 k_F^2}{t_\perp^2} \int_{k_F}^{\Lambda_{\mathrm{bil}}} d\mathbf{k} \frac{|\mathbf{k}|}{\epsilon_{\mathbf{k}}}, \tag{34}$$

where $\Lambda_{\mathrm{bil}} = t_\perp/v_{\mathrm{F}}$ is a high momentum cutoff above which the assumption that $v_F k \ll t_\perp$ ceases to be valid. The integral in this expression has a logarithmic dependence on Λ_{bil}, similar to the logarithmic divergences which characterize the charge susceptibility of a bilayer.[31]

As in the case of the single layer, when we insert Eq. (34) into the expression for the shift in the phonon frequency, we find an term which is independent of the number of carriers, given by k_F. Taking it out, and neglecting logarithmic corrections, we find

$$\delta\omega_{\mathbf{Q}}^{\mathrm{bilayer}} \propto -\left(\frac{\partial t_0}{\partial l}\right)^2 \frac{n}{M_C \omega_{\mathbf{Q}} t_\perp}. \tag{35}$$

We expect a similar dependence for other multilayer systems, as the main ingredient in this estimate, the changes in the low energy density of states in the two sublattices in each graphene layer, is independent of the number of layers in the stack. If the carrier density differs significantly among the layers,[32] we expect that phonons at each layer will be shifted by a quantity which depends on the local charge. Note that a crossover to a shift typical of single layer graphene will take place at $\omega_{\mathbf{Q}} \sim t_\perp$. A similar crossover will occur if $\mu \sim t_\perp$.

A bilayer system can show a gap in the electronic spectrum, when an applied field or chemical doping breaks the symmetry between the two layers. In this case, the electronic states close to the gap are mainly localized in one of the layers. The polarizability shown in the diagram in Fig. 1 acquires a layer index, and is different in the two layers. Hence, we expect that the in-plane phonons in each layer experience a different frequency shift. In a first approximation, the phonons in the layer where the states at the Fermi energy have highest weight show the largest shift. Using dimensional arguments similar to those leading to Eq. (32), we expect that, when the Fermi wavevector is much smaller than

the wave vector at the center of the band of the biased bilayer $k_F \ll k_0 \approx \Delta / v_F$ the factor $n \sim k_F^2$ in Eq. (35) is replaced by $k_0^2 \propto \Delta^2$.

The full dynamical response of a bilayer under a perpendicular applied field is quite complex when the chemical potential is close to the gap edges,[33] with an anomalously large imaginary part. Hence, low energy phonons in a biased bilayer should be significantly damped.

V. CONCLUSIONS

We have analyzed the effect of a finite concentration of carriers on the frequency shift of phonons in electrically doped graphene samples. We have not considered changes due to modifications of the force constants, associated to distortions of the σ bonds. The analysis presented here shows that the shift in the optical phonon frequencies in electrically doped graphene samples can be observed in Raman experiments,[8–10] and it can be used to estimate the carrier density, or alternatively, the strength of the electron-phonon coupling. Notice that in an ordinary 2D electron gas the density of states (and charge susceptibility) depends only on the electronic effective mass m^* and is independent of the electronic density. Therefore, for an ordinary 2D electron gas the frequency shift is essentially uniform and independent of disorder. For Dirac fermions, however, because of the effective Lorentz invariance in the continuum limit, we can write an equivalent of Einstein's relation between energy and mass: $\mu = m^* v_F^2$ (where the Fermi-Dirac velocity now plays the role of speed of light), indicating that the effective mass is energy dependent and vanishes at the Dirac point ($\mu = 0$). Therefore, the effect described here does not work in an ordinary 2D electron gas.

Another interesting consequence of Eq. (24) is that the Raman shift should be larger close to extended effects such as edges, dislocations and cracks.[8–10] The reason for that is the so-called self-doping effect discussed in great detail in Ref. 2: because of the poor screening properties of Dirac fermions, the Coulomb interactions remain long ranged and an electrostatic potential builds up at the edges of the system, shifting the position of the surface states, and reducing the charge transfer to or from them. In this case the system, in order to maintain charge neutrality, can transfer charge to/from extended defects. This charging transfer is only halted when the charging energy of the edges is compensated by the kinetic energy of the electrons. Thus, extra charge and a large density of states can be found at the edges of samples. In this case, according to Eq. (24), the Raman shift should change as a function of the distance from the sample edges (being larger at the edge). We have estimated that for edges of size $0.1-1$ μm the charge transfer is order of $10^{-4}-10^{-5}$ electrons per carbon ($\delta n \approx 10^{11}-10^{12}$ electrons per cm^{-2}) and hence the Raman shift is also of the order of a few wavenumbers but slightly larger than the effect produced by bulk disorder. We also notice that this effect is not possible in the ordinary 2D electron gas because screening leads to a uniform charge distribution.

The shift of phonons with energies comparable or larger than the Fermi energy is determined by the dynamic electronic response function, which is significantly different from the static one. In this regime, the shift changes when $\mu \approx \omega_{\mathbf{Q}}/2$, and vanishes at $\omega_{\mathbf{Q}} \gg \mu$.

Our results also suggest that the shift in phonon frequencies has a different dependence on carrier density in single layer and many layer systems, Eqs. (24) and (35). For a given carrier density, the shifts in phonon frequencies should scale as $\delta\omega_{\mathbf{Q}}^{1L} \approx \delta\omega_{\mathbf{Q}}^{2L} t_0 \sqrt{n_\Omega}/t_\perp$. Assuming that $t_\perp/t_0 \approx 0.1$, the shift in a bilayer should be smaller than in a single layer sample with the same carrier concentration. This is consistent with experimental results which show that the phonon frequencies in single layer systems are consistently lower than in samples with many layers.[8–10] The difference between a single layer and many layer systems is due to the fact that the low energy electronic wavefunctions has a reduced weight on the sites connected to other layers. Hence, it depends on the stacking order, and the shift is different in samples with regions with rhombohedral structure $(123123\cdots)$.[34] In systems where the charge distribution among the layers is not uniform, we expect that the shift of the phonons in different layers is also different, leading to a splitting of the single layer phonon frequencies. Similar effects may also occur in bulk graphite.[35]

In summary, we have studied the effect of electronic inhomogeneities in the phonon spectrum of Raman active modes in graphene. We have shown that the electron-phonon coupling leads to a shift of the optical phonon frequency that is dependent on local electronic density. We argue that the frequency shift is larger at the edges than in the bulk of graphene and its value is of order of a few wavenumbers. These results have their origin on the Dirac-like nature of the quasiparticles in these materials and hence do not have an analog in the ordinary 2D electron gas.

ACKNOWLEDGMENTS

We thank N. M. R. Peres for many level-headed comments. Discussions with K. Ensslin, A. Ferrari, A. Geim, B. Goldberg, D. Graf, Philip Kim, F. Mauri, A. Pinczuk, and A. Swan, are acknowledged. A.H.C.N. was supported through NSF Grant No. DMR-0343790. F.G. acknowledges funding from MEC (Spain) through Grant No. FIS2005-05478-C02-01 and the European Union Contract 12881 (NEST).

APPENDIX: ANALYTICAL MODEL FOR THE IN PLANE PHONONS IN GRAPHENE

1. The model

The simplest model for the phonons of a single graphene plane includes only nearest neighbor central forces,[24] following similar models for the diamond lattice:[25]

$$\mathcal{H} = \sum_{m,n} \frac{p_{mn}^2}{2M} + \sum_{k,l;m,n} \frac{M\omega_0^2[(\mathbf{a}_{kl} - \mathbf{a}_{mn})(\mathbf{r}_{kl} - \mathbf{r}_{mn})}{2}, \tag{A1}$$

where the indices k,l and m,n label lattice sites which are nearest neighbors. The three possible orientations of the

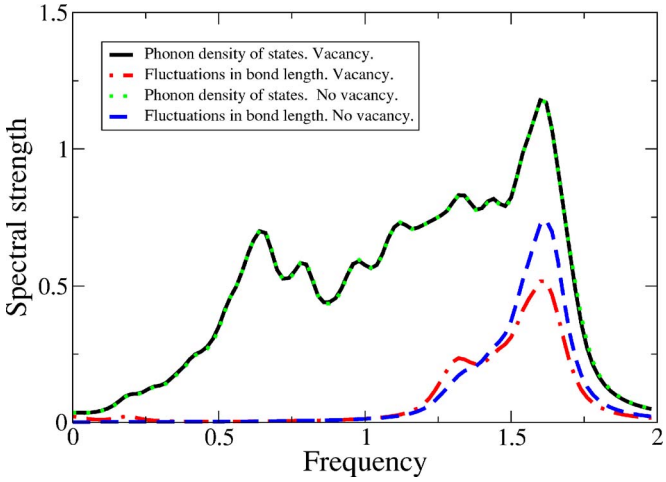

FIG. 5. (Color online) Phonon density of states and spectral function of bond fluctuations. Continous line (black): phonon density of states with vacancy; dashed-dotted line (red): fluctuations in bond length with vacancy; dotted line (green): phonon density of states without vacancy; dashed line (blue): fluctuations in bond length without vacancy.

bonds attached to a given site, m,n, allows us to define three unit vectors, $\mathbf{b}^i_{mn}, i=1,2,3$. We define the displacement of the atom at site m,n, $\mathbf{r}_{mn}$ by the three projections $x^i_{mn}=\mathbf{b}^i_{mn}\mathbf{r}_{mn}$. These numbers satisfy $\Sigma_{i=1,2,3}x^i_{mn}=0$. The model contains a single parameter, $\omega_0=\sqrt{K/M}$, where K is the spring constant of the bonds, and M is the mass of the carbon atom.

The equations of motion are

$$\omega^2 x^i_{mn} = \omega_0^2\left[(x^i_{mn}-x^i_{m'n'})-\frac{1}{2}\sum\nolimits_{j\neq i}(x^j_{mn}-x^j_{m''n''})\right], \tag{A2}$$

where the indices $m'n'$ and $m''n''$ label sites which are nearest neighbors to site mn (see Fig. 2) We now define the variable

$$b_{mn} = x^1_{m'n'} + x^2_{m''n''} + x^3_{m'''n'''} \tag{A3}$$

using the displacements at the three sites connected to site mn (see Fig. 3). In terms of these variables, the equations of motion (A2), can be written as

$$\omega^2 b_{mn} = \frac{3}{2}\omega_0^2 b_{mn} + \frac{1}{2}\omega_0^2 \sum_{m'n'} b_{m'n'}, \tag{A4}$$

where $m'n'$ label the three sites connected to site mn. The calculation of the phonon eigenstates is reduced to a tight binding model with one orbital per site in the honeycomb lattice. From Eq. (A4), we obtain two bands

$$\frac{\omega_{\mathbf{k}}}{\omega_0} = \sqrt{\frac{3}{2} \pm \frac{1}{2}\sqrt{3+2[\cos(\mathbf{k}\cdot\mathbf{a}_1)+\cos(\mathbf{k}\cdot\mathbf{a}_2)+\cos(\mathbf{k}\cdot\mathbf{a}_3)]}}, \tag{A5}$$

where $\mathbf{a}_1$, $\mathbf{a}_2$ are the unit vectors of the honeycomb lattice, and $\mathbf{a}_3=\mathbf{a}_1-\mathbf{a}_2$. From the knowledge of the variables b_{mn} the equations of motion (A2) can be written as

$$\omega^2 x^1_{kl} = \frac{3\omega_0^2}{2}(x^1_{kl}-x^1_{mn}) - \frac{\omega_0^2}{2}b_{mn},$$

$$\omega^2 x^1_{mn} = \frac{3\omega_0^2}{2}(x^1_{mn}-x^1_{kl}) - \frac{\omega_0^2}{2}b_{kl}. \tag{A6}$$

From these equations the atomic displacements can be deduced from the set $\{b_{mn}\}$.

The equations of motion (A2) assume that all the variables b_{mn} are different from zero. When $b_{mn}=0$, Eq. (A6) admit two additional solutions for $\omega^2=0$, and $\omega^2=3\omega_0^2/2$. The bands obtained in Eq. (A5) correspond to the longitudinal acoustical (LA) and longitudinal optical modes (LO). The two additional flat bands obtained when $b_{mn}=0$ describe the transverse acoustical (TA) and transverse optical (TO) modes. The phonon bands are shown in Fig. 3. The existence of a flat TA band at $\omega=0$ reflects the band that the honeycomb lattice can be distorted without changing the distance between nodes. These deformations do not have an energy cost in a nearest neighbor central forces model described in Eq. (A1). The velocity of sound of the LO modes is $v_s=(\omega_0 a)/(2\sqrt{2})$, where a is the lattice constant.

2. Defects

The mapping to a scalar tight binding model of the Hamiltonian in Eq. (A1) can be extended to lattices with defects. We describe the defect as the absence of bonds. Hence, an atom near a defect is attached to fewer neighbors than one at the bulk. This implies that the condition $\Sigma x^i_{mn}=0$ is no longer satisfied. We can take this into account by defining a new variable at the sites near the defect $a_{mn}=\Sigma'_i x^i_{mn}$, where the sum is restricted to the bonds which remain intact.

a. Zigzag edge

The atoms at a zigzag edge are connected by only two bonds to the rest of the lattice. We define the variable b_{mn} using the displacements of the two nearest neighbor atoms to the edge atom mn. The atomic displacements used to define the variables a_{mn} and b_{mn} are sketched in Fig. 4. The equations of motion for the variables a_{mn} and b_{mn} when the indices mn label an atom at the edge become

$$\omega^2 a_{mn} = \frac{\omega_0^2}{2}(a_{mn}-b_{mn}),$$

$$\omega^2 b_{mn} = \frac{3\omega_0^2}{2}b_{mn} - \frac{\omega_0^2}{2}\sum_{m'n'} b_{m'n'} - \frac{\omega_0^2}{2}a_{mn},$$

$$\omega^2 b_{m'n'} = \frac{3\omega_0^2}{2} b_{m'n'} - \frac{\omega_0^2}{2} \sum_{m''n''} b_{m''n''} - \frac{\omega_0^2}{2} a_{mn}, \quad \text{(A7)}$$

where the indices $m'n'$ label the sites which are the nearest neighbors of the vacancy, and $m''n''$ stand for the next nearest neighbors. The equations of motion for the remaining atoms are not changed from Eq. (A4).

Thus, the equations of motion of the atoms can be mapped onto a tight binding model. The only difference with the bulk case is that the description of the displacements of the atoms at the boundary require the definition of two effective orbitals. The position of the effective orbital level a_{mn} at the edge, $\omega_0^2/2$, is lower than that for the variable $b_{mn}, (3\omega_0^2)/2$. This reflects the fact that atomic fluctuations are enhanced at the edge.

b. Vacancy

As in the case of an atom at a zigzag edge, the three atoms near a vacancy are connected by bonds to two nearest neighbors only. As in the previous case, a new variable, $a_{mn} = \Sigma_i' x_{mn}^i$ needs to be defined at these three sites. The equations of motion for the variables a_{mn} and b_{mn} are those in Eq. (A7).

The phonon density of states in clusters with and without vacancies, and the spectral strength of the bond length fluctuations, in the bulk and near a vacancy are shown in Fig. 5. Contrary to what happens for the π electronic band, the phonons are not too disturbed near a vacancy, although some shift of spectral strength to lower energies takes place.

[1] K. S. Novoselov, A. K. Geim, S. V. Morozov, D. Jiang, Y. Zhang, S. V. Dubonos, I. V. Gregorieva, and A. A. Firsov, Science **306**, 666 (2004).
[2] N. M. R. Peres, F. Guinea, and A. H. Castro Neto, Phys. Rev. B **73**, 125411 (2006).
[3] V. P. Gusynin and S. G. Sharapov, Phys. Rev. Lett. **95**, 146801 (2005).
[4] K. S. Novoselov, A. K. Geim, S. V. Morozov, D. Jiang, M. I. Katsnelson, I. V. Grigorieva, S. V. Dubonos, and A. A. Firsov, Nature (London) **438**, 197 (2005).
[5] Y. Zhang, Y.-W. Tan, H. L. Stormer, and P. Kim, Nature (London) **438**, 201 (2005).
[6] W. Shockley, *Electrons and Holes in Semiconductors: With Applications to Transistor Electronics* (Krieger, Melbourne, FL, 1976).
[7] S. V. Morozov, K. S. Novoselov, M. I. Katsnelson, F. Schedin, L. A. Ponomarenko, D. Jiang, and A. K. Geim, Phys. Rev. Lett. **97**, 016801 (2006).
[8] A. C. Ferrari, J. C. Meyer, V. Scardaci, C. Casiraghi, M. Lazzeri, F. Mauri, S. Piscanec, D. Jiang, K. S. Novoselov, S. Roth, and A. Geim, Phys. Rev. Lett. **97**, 187401 (2006).
[9] A. Gupta, G. Chen, P. Joshi, S. Tadigadapa, and P. C. Eklund, cond-mat/0606593 (unpublished).
[10] D. Graf, F. Molitor, K. Ensslin, C. Stampfer, A. Jungen, C. Hierold, and L. Wirtz, cond-mat/0607562 (unpublished).
[11] J. Yan, Y. Zhang, P. Kim, and A. Pinczuk (unpublished).
[12] A. Geim *et al.* (unpublished).
[13] E. Fradkin, Phys. Rev. B **33**, 3257 (1986).
[14] E. McCann, K. Kechedzhi, V. I. Falko, H. Suzuura, T. Ando, and B. L. Altshuler, Phys. Rev. Lett. **97**, 146805 (2006).
[15] A. F. Morpurgo and F. Guinea, Phys. Rev. Lett. **97**, 196804 (2006).
[16] D. V. Khveshchenko, Phys. Rev. B **74**, 161402(R) (2006).
[17] K. Ziegler, cond-mat/0604537 (unpublished).
[18] K. Nomura and A. H. MacDonald, cond-mat/0606593 (unpublished).
[19] I. L. Aleiner and K. B. Efetov, cond-mat/0607200 (unpublished).
[20] A. Altland, cond-mat/0607247 (unpublished).
[21] L. Wirtz and A. Rubio, Solid State Commun. **131**, 141 (2004).
[22] R. O. Dillon, I. L. Spain, and J. W. McClure, J. Phys. Chem. Solids **38**, 635 (1977).
[23] N. B. Brandt *et al.*, *Semimetals 1: Graphite and its Compounds* (North-Holland, Amsterdam, 1988).
[24] F. Guinea, J. Phys. C **14**, 3345 (1981).
[25] D. Weaire and R. Alben, Phys. Rev. Lett. **29**, 1505 (1972).
[26] Kenneth W.-K. Shung, Phys. Rev. B **34**, 979 (1986).
[27] J. González, F. Guinea, and M. A. H. Vozmediano, Nucl. Phys. B **424 [FS]**, 595 (1994).
[28] J. González, F. Guinea, and M. A. H. Vozmediano, Phys. Rev. B **59**, R2474 (1999).
[29] T. Ando, J. Phys. Soc. Jpn. **75**, 074716 (2006).
[30] B. Wunsch, T. Stauber, F. Sols, and F. Guinea, cond-mat/0610630 (unpublished).
[31] J. Nilsson, A. H. Castro Neto, N. M. R. Peres, and F. Guinea, Phys. Rev. B **73**, 214418 (2006).
[32] F. Guinea, cond-mat/0611185 (unpublished).
[33] T. Stauber, N. M. R. Peres, F. Guinea, and A. H. Castro Neto, cond-mat/0611468 (unpublished).
[34] F. Guinea, A. H. Castro Neto, and N. M. R. Peres, Phys. Rev. B **73**, 245426 (2006).
[35] S. Y. Zhou, G.-H. Gweon, and A. Lanzara, Ann. Phys. (N.Y.) **321**, 1730 (2006).